Tidal Rectification and Mass Transport over a Shelf Break: A Barotropic Frictionless Model

PIERRE GARREAU AND ROBERT MAZE

Laboratoire d'Oceanographie Physique, Universite de Bretagne Occidentale, Brest, France

(Manuscript received 12 April 1990, in final form 16 July 1991)

ABSTRACT

A depth-independent model for the tidal rectification process is developed in order to explain the residual Eulerian velocity observed at the top of a shelf edge. An approximation of the nonlinear equations for an inviscid ocean is considered.

It is found that the Lagrangian mean current vanishes if the geostrophic contours are closed. Exact conservation of the potential vorticity along a water column trajectory indicates that the model and its approximations are valid. Quantitative results are shown for an idealized shelf break (constant bottom slope). Finally, a realistic transect is considered in the north of the Bay of Biscay. The residual and fortnightly tide behavior is examined.

1. Introduction

a. Motivation

For many years, the continental slope area around Chapel Bank (47°30'N, 7°30'W) in the northeast Atlantic has been a subject of interest. The semidiurnal tide is the major feature of the dynamics of the zone. Various sets of data, as well as numerical models, show that tidal currents can reach 0.3 m s^{-1} during neap tides and 0.7 m s^{-1} at spring tides near the shelf break along the 200-m isobath.

Analysis of measurements shows that the mean current along the crest of the slope can reach values 10% or 20% of the instantaneous current amplitude. Along the 200-m isobath, the mean currents flow northwestward at speeds in the range of 5–13 cm s^{-1} (Fig. 1). On the whole, direction of flow is parallel to the shelf break and confined to the top of the slope, as shown by the difference between the values of current speed in P_1 and P_2 (during the ONDINE85 Experiment in October–November 1985). In P_1 (Fig. 1) depth is 173 m and current velocity is 8.5 cm s^{-1}, whereas in P_2 it is only of 3.5 cm s^{-1} for a depth of 168 m. These two points are as close as one-half nautical mile. Another example of the specific localization of the phenomenon is given by moorings 64 and 65 where both amplitude and direction of the current vary considerably.

Characteristic of the shelf break is a variation in depth from 4500 to 200 m over a length of 60 km. The average slope is about 7% but reaches a maximum of 14% about 1500 m deep. Along the 200-m isobath, which is the presumed area of internal tide generation (Pichon and Maze 1990) and of the maximal observed residual current, the slope is 4%. The nondimensional parameter indicating nonlinearity is the ratio of the tidal excursion, L_M, over the horizontal topographic length scale, L_T. If U is the current amplitude of the tide, ω the frequency, and H the total depth, these length scales are therefore defined by

$$L_T = H(x) \Big/ \frac{dH}{dx} \tag{1}$$

$$L_M = \frac{U(x)}{\omega}. \tag{2}$$

Length scales L_M and L_T have been calculated considering a tidal current with an amplitude of 0.40 m s^{-1} at a depth of 200 m and assuming HU constant. This ratio shows a sharp maximum of 0.35 at the 200-m isobath, confirming the dynamical importance of that area (Fig. 2). The nonlinearities decrease acutely on the shelf, and 5 km inshore the ratio is only 0.03. Mooring P_1 is located near the maximum nonlinearity.

Thus, we expect a tidal rectification process at the top of the shelf break. Other processes may also be involved and contribute to form the mean current. Among those processes are local adjustment to an oceanic forcing (pressure or density gradient) and the consequence of a geostrophic balance associated with a front in this transition region. The same experimental area has been examined in regards to internal waves (Pichon and Mazé 1990) and slope currents (Pingree and Lecann 1989).

Corresponding author address: Dr. Pierre Garreau, IFREMER Centre de Brest, B.P. 70, Plouzane 29280, France.

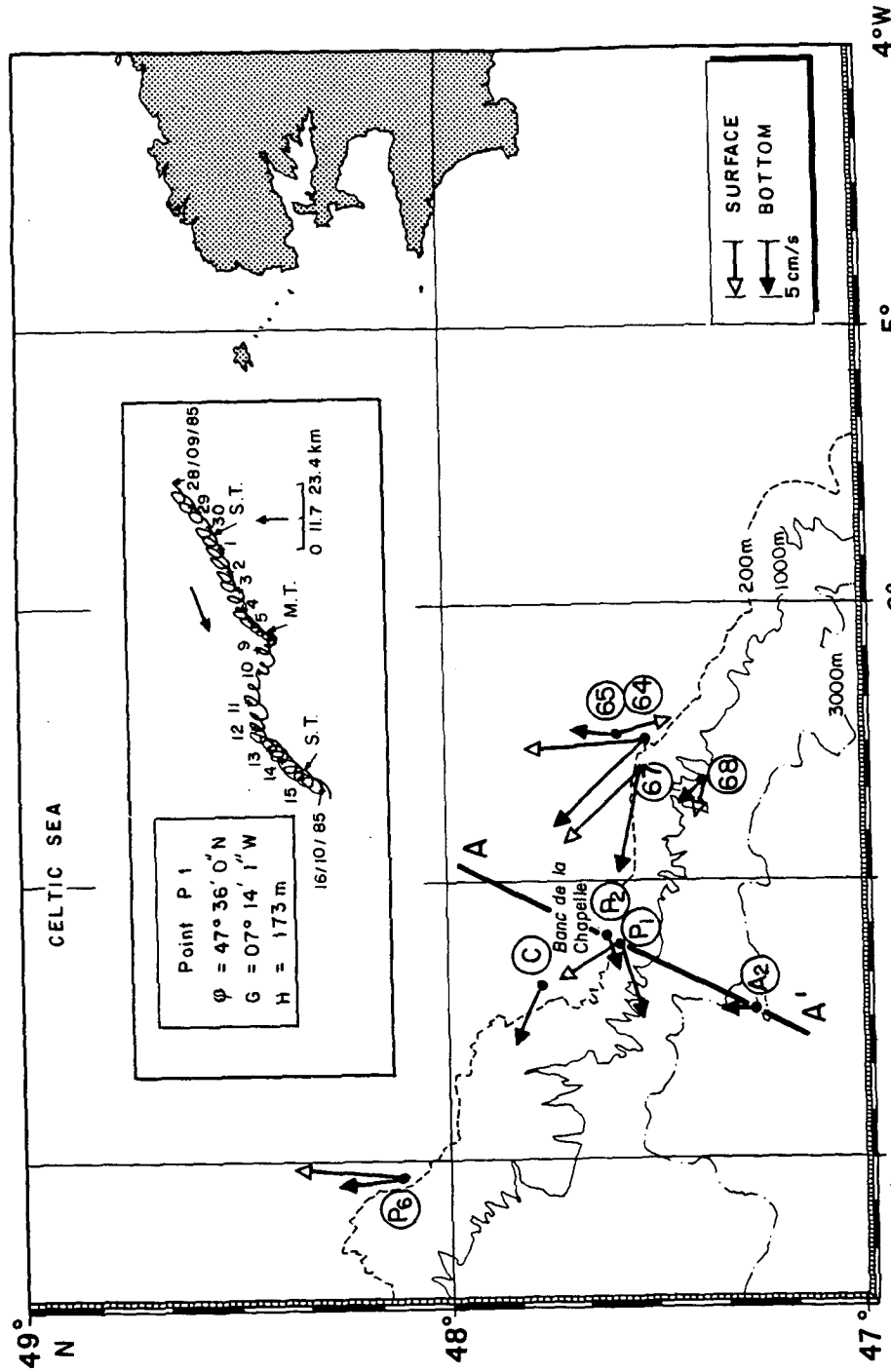

FIG. 1. Eulerian mean currents in surface layer (0–30 m deep: white arrow) and in bottom layer (>100 m deep: black arrow) in the vicinity of the shelf break in the north of the Bay of Biscay. Moorings 64–68 are data from the MBA, Plymouth, (Pingree). Moorings C and B (ENVAT81), and A2, and P1–P6 (ONDINE85) are data from the EPSHOM and the University de Bretagne Occidentale, Brest. Progressive vector diagram in the bottom layer (112 m deep) at P_1 for 21 days in September and October 1985. Note the effects of neap tide (at 8 Oct 1985) and spring tides (at 30 Sep 1985 and at 15 Oct 1985).

b. Previous studies

Tidal rectification theories have been developed to explain the existence of residual currents in coastal environments. At shallow depths, topographic irregularities and effects of nonlinear terms (friction and advection) are important. Moreover, energy transfer between the fundamental tidal frequency and higher harmonics, or the residual field (i.e., integrated over one tidal period), cannot be omitted.

The existence of residual motion on sandbanks and islands, capes and bays, and idealized bottom slopes is often discussed in the literature. In a review article, Zimmerman (1981) emphasizes the importance of scaling, mainly with regards to the ratio of tidal excursion to a horizontal lengthscale. Robinson (1981, 1983) lists the different processes involved and how different scientists have dealt with the question.

Harmonic separation and truncation allow, in some simple geometric cases, solution of the problem analytically. Huthnance (1973) has applied that method to a rectilinear sandbank. Loder (1980) has improved the method and applied it to Georges Bank.

The study of relative vorticity reveals, usually qualitatively, the existence of both eddies and, as a consequence, residual currents. By losing any reference to a free surface behavior in that transformation, it is then possible to study the effect of any topography on residual current (Pingree and Maddock 1979, 1980a,b; Pingree and Mardell 1987). Relative vorticity equations can also be solved by using Fourier transformations to connect the spectral properties of topography to those of the mean current (Zimmerman 1980). However, such a pattern only applies to a series of sandbanks.

More recently this idea has been used to describe exactly the vorticity over a sinusoidal topography of small amplitude (Maas et al. 1987). A perturbation method is used rather than a harmonic truncation. The extreme case of steplike topography is considered, and the roles of friction and vortex stretching in generating residual vorticity are shown.

Interestingly, the Langrangian mean current generated by a simple wave in a rotating ocean of variable depth is the solution of the linearized unforced geostrophical motion (Moore 1970). This implies that the eventual mass transport has to follow the geostrophical contours. Huthnance (1981) shows that the latter result is not affected by the strength of a weak bottom friction.

2. Physical background and hypothesis

a. Basic equation

For local study we assume a semidiurnal tidal wave propagating from the abyssal plain with a normal incidence to a rectilinear shelf break. A right-handed Cartesian coordinate system (x, y, z) is used with the

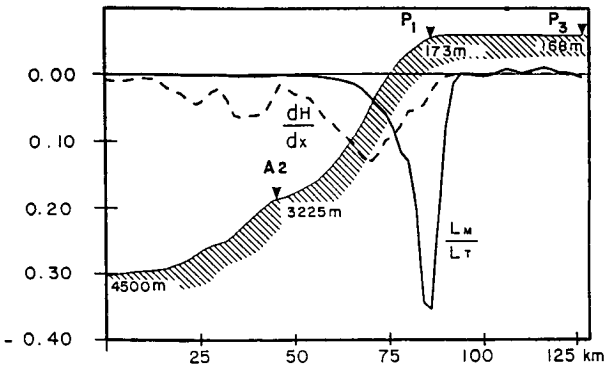

FIG. 2. Depth profile along the transect A'–A. The bottom slope (dotted) has a maximum of −14% around 1500-m depth. Nonlinearities have a very sharp maximum around 200-m depth (ratio L_T/L_R for $H_d u_d = 80\ \mathrm{m^2\ s^{-1}}$) (solid).

x axis perpendicular to isobaths in the direction of decreasing depth. The y axis is oriented with the shallow area to its right. Assuming that all y gradients vanish, the vertically integrated equations of the motion become

$$\frac{\partial u^*}{\partial t} + u^* \frac{\partial u^*}{\partial x} - fv^* = -g\frac{\partial \zeta^*}{\partial x} - ru^*$$

$$\frac{\partial v^*}{\partial t} + u^* \frac{\partial v^*}{\partial x} + fu^* = -rv^*$$

$$\frac{\partial[(H + \zeta^*)u^*]}{\partial x} = -\frac{\partial \zeta^*}{\partial t}. \qquad (3)$$

For the remainder of the paper, the asterisk variables represent nonlinear solutions for physical quantities or their approximations. Here u^* is on the x axis, v^* is the y-axis nonlinear velocity component, and ζ^* is the free-surface perturbation. Also, f is the Coriolis parameter, g the gravitational acceleration, r a friction coefficient dependent on the x coordinate, and $H(x)$ the depth.

b. Harmonic separation and truncation

Motion can be decomposed into a sum of mean (time averaged) motion and a tidal contribution and its harmonics. Strictly speaking, each period should be simultaneously solved but usually the series are truncated after the first harmonic. Velocities and the sea surface elevation can therefore be expressed as

$$(u^*, v^*, \zeta^*) = (\tilde{u} + \bar{u}, \tilde{v} + \bar{v}, \tilde{\zeta} + \bar{\zeta}). \qquad (4)$$

The overbar represents time averaging over a tidal period and indicates time-independent or residual variables. The tilde represents the contribution of the M_2 oscillating motion. Introducing (4) in (3) gives:

Tidal frequency

$$\frac{\partial \tilde{u}}{\partial t} - f\tilde{v} = -g\frac{\partial \tilde{\zeta}}{\partial x} - \left[r\tilde{u} + \tilde{u}\frac{\partial \bar{u}}{\partial x} + \bar{u}\frac{\partial \tilde{u}}{\partial x}\right]$$

$$\frac{\partial \tilde{v}}{\partial t} + f\tilde{u} = -\left[r\tilde{v} + \tilde{u}\frac{\partial \bar{v}}{\partial x} + \bar{u}\frac{\partial \tilde{v}}{\partial x}\right]$$

$$\frac{\partial H\tilde{u}}{\partial x} = -\frac{\partial \tilde{\zeta}}{\partial t} - \left[\frac{\partial \tilde{\zeta}\bar{u}}{\partial x}\right]. \qquad (5)$$

When we neglect bracketed terms in (5), the solutions are very simple. In appendix A, the form of the exact solution and its classical approximation are developed. It is a Poincaré wave that is partially reflected and transmitted over a slope. The crests are almost parallel to the isobaths and the hodograph describes an ellipse whose major axis is normal to the shelf break:

Residual motion

$$\overline{\tilde{u}\frac{\partial \tilde{u}}{\partial x}} - f\bar{v} = -g\frac{\partial \bar{\zeta}}{\partial x} - \left[\bar{u}\frac{\partial \bar{u}}{\partial x} + r\bar{u}\right]$$

$$\overline{\tilde{u}\frac{\partial \tilde{v}}{\partial x}} + f\bar{u} = -\left[\bar{u}\frac{\partial \bar{v}}{\partial x} + r\bar{v}\right]$$

$$\frac{\partial(\overline{\tilde{\zeta}\tilde{u}})}{\partial x} + \frac{\partial(H\bar{u})}{\partial x} = 0. \qquad (6)$$

The first term in each equation of (6) comprises forcing terms (the Reynolds stress) for the residual motion; they depend on tide propagation. If we neglect residual self-advection and friction [i.e., the bracketed term in (6)], then the mass conservation gives

$$\bar{u} = -\frac{\overline{\tilde{\zeta}\tilde{u}}}{H}.$$

The residual Eulerian current is then a function of the mean energy flux $\bar{\phi}_U$ (appendix A):

$$\bar{u} = -\frac{\overline{\phi_U}}{\rho g H^2}.$$

While the $\tilde{u}$ current is almost proportional to H^{-1}, the conservation of energy induces a residual current proportional to H^{-2}. For a wave propagating from the abyssal plain, the cross-shelf residual current is directed toward that plain. In the Celtic Sea, over the Chapel Bank, the energy flux entering the continental shelf is about 400 kW m^{-1}. The residual current $\bar{u}$ is then 1×10^{-3} m s^{-1} at a depth of 200 m. This value is so small that it is less than current-meter resolution.

In the second momentum equation of (6), the forcing term can be evaluated by using the relation describing wave propagation (appendix A) and can also be expressed in terms of energy flux:

$$\overline{\tilde{u}\frac{\partial \tilde{v}}{\partial x}} = \frac{f\overline{\phi_U}}{\rho g H^2} = -f\bar{u}.$$

The second and third equation in (6) are consistent, and the first momentum equation has two unknown quantities $\bar{v}$ and $\bar{\zeta}$ (after removing the bracketed terms). Thus, the equations are not closed. This is a direct consequence of the rectilinear shelf-break assumption because it is implicit that $\bar{v}$ and $\bar{\zeta}$ are not set when $x = \pm\infty$. Any residual current in geostrophic balance with the surface slope is possible but not determined. Harmonic separation and truncation provide an incomplete approximation of the inviscid equation. The result is a geostrophic balance to which the mean contribution of the quadratic terms is added. Accepted approximations, although valid, have lead to a problem of geostrophic degeneracy, which is widely described in the literature (Pedlosky 1979). It is obvious that only by including the dynamical secondary effects, like advection or friction, can we proceed. Thus, by accounting for friction, Huthnance (1973) and Loder (1980) have been able to remove the degeneracy.

c. *Results with friction*

The tidal rectification process, developed first by Huthnance (1973) and improved by Loder (1980), is based on the effect of friction. A sandbank generates relative vorticity by vortex stretching of the fluid that moves on top of it. Dissipation, which is stronger over smaller depth, causes distortion in the vorticity advection. The result is the generation of a residual relative vorticity and consequently a mean current along the bank when the water column is submitted to an oscillatory tidal motion.

In terms of currents, friction introduces a supplementary phase lag between $\tilde{u}$ and $\tilde{v}$. Thus, they are no longer in quadrature, and the forcing term $\overline{(\tilde{u}\partial\tilde{v}/\partial x)}$ in the y-residual momentum equation of (6) does not vanish. To balance this term, a residual current $\tilde{v}$ should be considered. To derive this, the procedure consists of first calculating the linear semidiurnal current that is perturbed by the friction ($\tilde{v}_r$). (The cross-isobath current is assumed unperturbed by friction or nonlinearities.) Second, the residual balance in the y direction leads to the evaluation of the residual current ($\bar{u}$ is negligible)

$$\bar{v} = \frac{1}{r}\overline{\tilde{u}\frac{\partial \tilde{v}_r}{\partial x}}.$$

Three classical parameterizations of r ($r = ku$; $r = ku/H$; $r = ku/H^2$; k const) are considered. In each case, it is possible to derive the residual current:

$$\bar{v} = \begin{cases} -\frac{1}{2}\dfrac{fH_d^2u_d^2}{\omega^2H^3}\dfrac{dH}{dx}, & r = k \\ -\dfrac{fH_d^2u_d^2}{\omega^2H^3}\dfrac{dH}{dx}, & r = k/H \\ -\frac{3}{2}\dfrac{fH_d^2u_d^2}{\omega^2H^3}\dfrac{dH}{dx}, & r = k/H^2. \end{cases} \qquad (7)$$

Huthnance (1981) observes that if friction is weak, the final result does not depend on the strength of friction but only on its parameterization. Rhines (1977) shows that a localized motion generates a zonal current in a beta plane. An extension to a topographic beta effect is carried out with a linear friction (ku). The same result as in both the Loder (1981) and the Huthnance (1973) procedures are found in the particular case of a periodic motion. Of course, these approximations are only a crude representation of frictional effects. More sophisticated friction laws have been developed (Wright and Loder 1988), but the physical process remains identical.

d. *Lagrangian concept*

Data quoted in the Introduction are given by current meters at a fixed position. Thus, estimated current values are Eulerian. Another appproach consists in following a water parcel and describing its instantaneous velocity according to its displacement. Let a water column be at the position (x_0, y_0) at time t_0. The calculation of its trajectory, when a rectilinear slope with normal incidence is considered, can be done by solving a differential equation:

$$\left.\begin{aligned} \frac{dX}{dt} &= u(X(x_0, t), t) \\ \frac{dY}{dt} &= v(X(x_0, t), t) \end{aligned}\right\} \tag{8}$$

where $X(t)$ and $Y(t)$ are positions of the water column at time t. The method used to solve (8) is a fourth-order Runge–Kutta formula. The Eulerian field used for computation is the linear field (appendix A). We consider different starting times t_0 for a column, relative to the position x_0; the trajectories vary as a function of these. Here $t_0 = 0, T/4, T/2, 3T/4$, where T is the tidal period, with $H(x_0) = 500$ m over a constant slope. After one tidal period the water column returns to the starting isobath. This result is logical since we consider Poincaré waves without any mass transport on the shelf. Whatever the starting time, the water columns have various negative y displacements in a range of 360–2000 m (Fig. 3). For a tidal period T, the mean Lagrangian current is defined as

$$\overline{v_L}(x_0, t_0) = \frac{Y(T) - Y(0)}{T}.$$

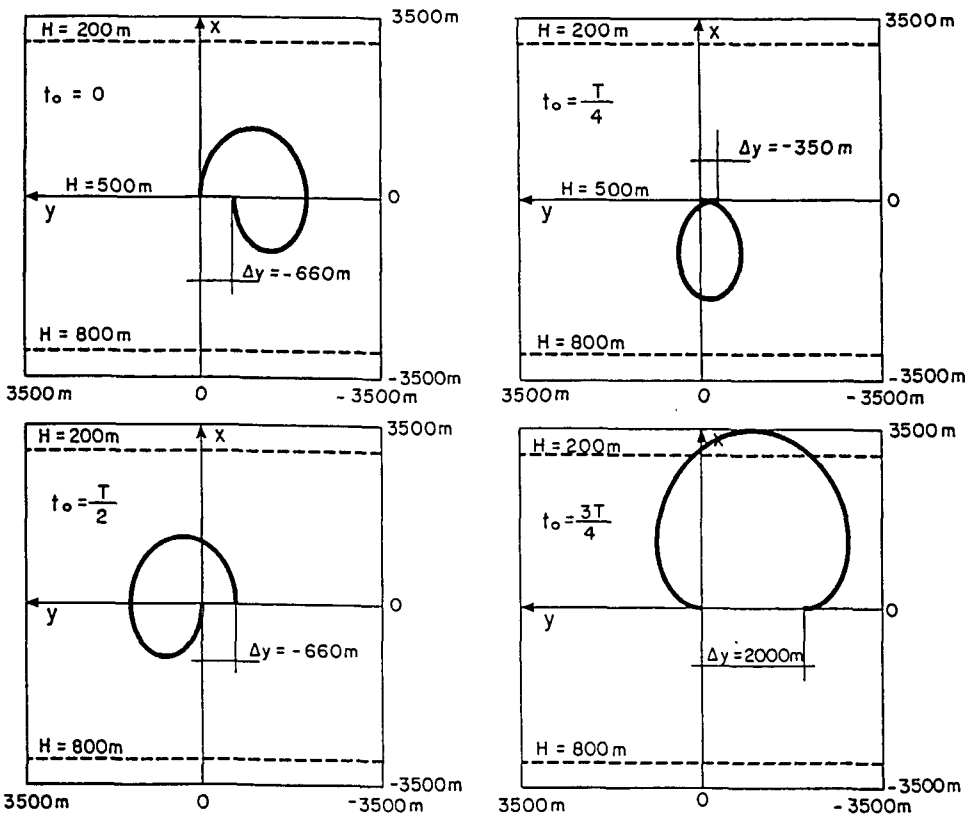

FIG. 3. Lagrangian trajectories resulting from the linear hypothesis. The bottom slope is constant ($dH/dx = -0.1$) and the position (0, 0) of the water column at various starting times ($t_0 = 0, T/4, T/2, 3T/4$) is 500 m deep.

For $H(x_0) = 500$ m, $dH/dx = -0.1$, and $H_d u_d = 80$ m^2 s^{-1}:

$$\bar{v}_L = 0.015 \text{ m s}^{-1}.$$

Often, the problem of passing from an Eulerian velocity field to a Lagrangian field occurs. The existence of such a relation for residual velocity has been commented on by Longuet-Higgins (1969) and Zimmerman (1979) when oscillating currents dominate. It is known that

$$\text{Lagrange} = \text{Euler} + \text{Stokes},$$

where Langrange is the mean Lagrangian velocity, Euler is the mean Eulerian velocity, and Stokes depends on wave propagation. Accordingly, calculation of the residual Lagrangian velocity for the linear approximation gives

$$\left.\begin{aligned} u_L(x_0, t_0 = 0) &= 0 \\ \bar{v}_L(x_0, t_0 = 0) &= -\frac{1}{2}\frac{f H_d^2 u_d^2}{\omega^2 H^3}\frac{dH}{dx} \end{aligned}\right\}. \quad (9)$$

Note that this result is only valid for sufficiently weak slope. For the linear approximation, the Eulerian mean current is equal to zero. Therefore, the residual Lagrangian velocity is exactly identical to the Stokes velocity.

3. Solving the nonlinear equations

Another way of removing the geostrophic degeneracy consists in solving the nonlinear equations without harmonic truncation and in analyzing the current thus obtained in terms of residual and tidal current. Our knowledge of the linear motion makes it possible to simplify the advection terms and leads to a simpler solution.

a. Basic equations

In order to approximate a nonlinear solution, we first linearize the two momentum equations of the system (3) by writing the advection terms in the form

$$u^* \frac{\partial}{\partial x} \approx u \frac{\partial}{\partial x}, \quad (10)$$

where u is a linearized solution for the cross-isobath current (A_2 or A_8). The strategy developed here consists in choosing a pseudo-Lagrangian coordinate transformation $x^*(x, t)$ that allows nonlinear currents to be derived from linear ones by

$$\begin{aligned} u^*(x, t) = u(x^*(x, t), t)) &= u_1(x^*)\cos(\omega t) \\ &\quad + u_2(x^*)\sin(\omega t) \\ v^*(x, t) = v(x^*(x, t), t)) &= v_1(x^*)\cos(\omega t) \\ &\quad + v_2(x^*)\sin(\omega t). \end{aligned} \quad (11)$$

Without loss of generality, x^* can be defined as a sum of space and time-dependent functions:

$$x^* = x + f_0(x, t) + f_1(x, t) + f_2(x, t) + \cdots + f_i(x, t) + \cdots.$$

Using (10) and introducing (11) in the equations governing the motion yields

$$\frac{\partial u(x^*, t)}{\partial x} + \left[\frac{\partial x^*}{\partial t} + u(x, t)\frac{\partial x^*}{\partial x}\right]\frac{\partial u(x^*, t)}{\partial x^*} - fv(x^*, t) = -g\frac{\partial \zeta^*}{\partial x} \quad (12)$$

$$\frac{\partial v(x^*, t)}{\partial x} + \left[\frac{\partial x^*}{\partial t} + u(x, t)\frac{\partial x^*}{\partial x}\right]\frac{\partial v(x^*, t)}{\partial x^*} + fu(x^*, t) = 0. \quad (13)$$

This useful transformation is one that causes the bracketed terms to vanish in (13) and builds a periodic solution for the currents as:

$$\left[\frac{\partial x^*}{\partial t} + u(x, t)\frac{\partial x^*}{\partial x}\right] = 0,$$

that is,

$$\left[\frac{\partial f_0}{\partial t} + \frac{\partial f_1}{\partial t} + \cdots + u + u\frac{\partial f_0}{\partial x} + u\frac{\partial f_1}{\partial x} + \cdots\right] = 0.$$

In order to derive the final result, the f_i functions are defined by a recurrent series:

$$\left\{\begin{aligned} \frac{\partial f_0}{\partial t} &= -u \\ \frac{\partial f_i}{\partial t} &= -u\frac{\partial f_{i-1}}{\partial x}. \end{aligned}\right. \quad (14)$$

If only the first two terms of the series are retained, the transformation becomes

$$x^* = x - \int_{t_0}^{t} u dt,$$

which is the opposite transformation to one that defines, to the same order, the Lagrangian y displacement

$$X(x_0, t) = x_0 + \int_{t_0}^{t} u dt.$$

The pressure gradient $(\partial \zeta^*/\partial x)$ can be determined by the first momentum equation (12). Finally, under a tidal Eulerian velocity field effect, a water column moving over the slope is submitted to vertical stretching. Water column trajectory and associated potential vorticity are fundamental aspects of tidal dynamics over a slope. Particularly, if no simplifications (e.g., linearization of the advection terms) are made, the potential vorticity should be constant along the trajectory. Thus, validity of the final solution can be verified.

b. Case of constant slope

For the sake of simplicity, the above theory is applied to a shelf break with a constant slope ($dH/dx = -a$) and for the linear currents A_{11} and A_{12} (cf. appendix A). Therefore, the linear currents over the slope are

$$u = \frac{H_d u_d \cos(\omega t)}{H_d[1 - (a/H_d)x]} \tag{15}$$

$$v = -\frac{f}{\omega}\frac{H_d u_d \sin(\omega t)}{H_d[1 - (a/H_d)x]}. \tag{16}$$

The origin of the coordinate system is taken at the rise of the continental slope (depth H_d). Straightforward algebra (appendix B) allows one to derive the x^* transformation as a series that converges for

$$\frac{2L_M}{L_T} \leqslant 1.$$

Thus, the useful pseudo-Lagrangian transformation is only available when nonlinearities are not dominant.

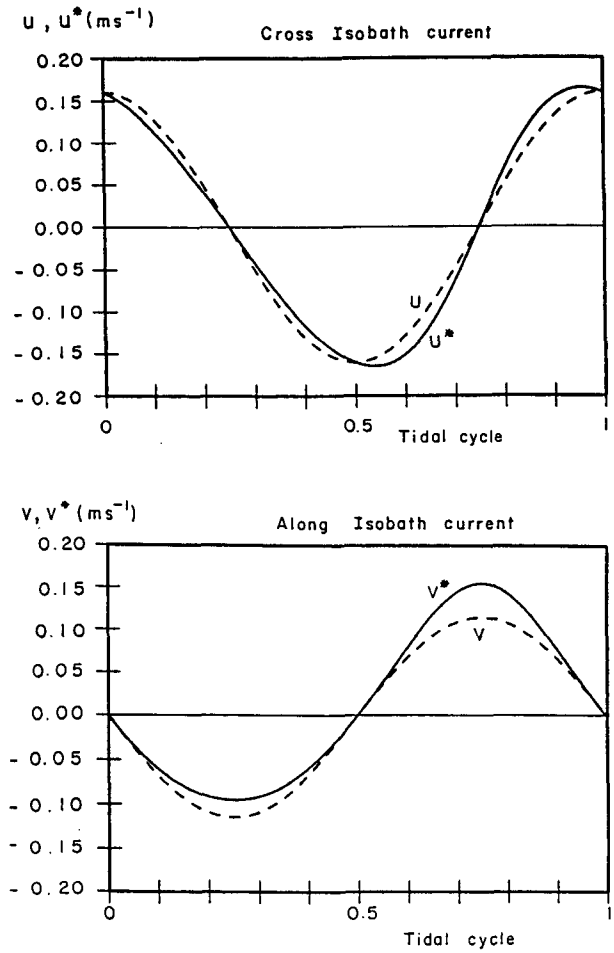

FIG. 4. Nonlinear (solid) and linear (dotted) tidal currents for a constant slope (H = 500 m and $H_d u_d$ = 80 m^2 s^{-1}, $dH/dx = -0.1$).

Let $H_d u_d$ = 80 m^2 s^{-1} and a = 0.1. Convergence is ascertained for depths equal to 340 m and more. Nonlinear solutions are (see appendix B)

$$u^*(x, t) = \frac{H_d u_d}{H(x)}\cos(\omega t)\left[1 + \frac{2aH_d u_d}{\omega H(x)^2}\sin(\omega t)\right]^{-1/2} \tag{17}$$

$$v^*(x, t) = -\frac{f}{\omega}\frac{H_d u_d}{H(x)} \times \sin(\omega t)\left[1 + \frac{2aH_d u_d}{\omega H(x)^2}\sin(\omega t)\right]^{-1/2}. \tag{18}$$

It is easy to verify that if (15) and (16) are acceptable solutions for linear motion, then u^* and v^* are solutions to a nonlinear approximation of the $0y$ momentum equation of (3). The potential vorticity equation is checked at the end of this chapter.

Nonlinear and linear tidal currents are compared (Fig. 4) for a depth H = 500 m, a mass flux $H_d u_d$ = 80 m^2 s^{-1} and a slope a = 0.1. The maxima of the cross-isobath current are slightly stronger and a deformation of the sinusoid is obvious but remains weak; therefore linearization of the advection terms is valid. The current $\overline{v^*}$ is clearly asymmetrical and the differences with linear behavior are more important. We observe a positive Eulerian residual current $\overline{v^*}$ that can be exactly evaluated by the time integration of (18):

$$\overline{v^*} = \frac{1}{2}\frac{faH_d^2u_d^2}{\omega^2H^3}\left[1 + \frac{15}{8}\left(\frac{aH_d u_d}{\omega H^2}\right)^2 + \cdots\right].$$

In the case of weak nonlinearities, only the first term in the bracket is retained, and thus the same result is obtained as for a linear friction law (ku). To this order of approximation, the Eulerian residual current found is also exactly the one that cancels the Stokes velocity in the linear approximation.

Considering $\zeta^* \ll H$, knowledge of the current allows one to calculate the trajectory of a column of fluid and its potential vorticity. The Lagrangian form of the linear (Q) and the nonlinear (Q^*) potential vorticity are

$$Q(X(x_0, t)) = \left[-\frac{f}{\omega}\frac{aH_d u_d \sin(\omega t)}{H(X)^2} + f\right]\Big/ H(X)$$

$$Q^*(X(x_0, t)) = \left\{-\frac{f}{\omega}aH_d u_d \sin(\omega t)\Big/ \left[H(X)^2\left(1 + \frac{2aH_d u_d \sin(\omega t)}{\omega H(X)^2}\right)^{3/2}\right] + f\right\}\Big/ H(X),$$

where X is the position of a water column along $0x$, and x_0 the starting position at t = 0. During a tide cycle, the trajectory of the nonlinear model is a closed curve (Fig. 5a). It is an ellipse described anticyclonically in which, the major-to-minor axis ratio equals ω/f. This confirms the disappearance of the Langrangian

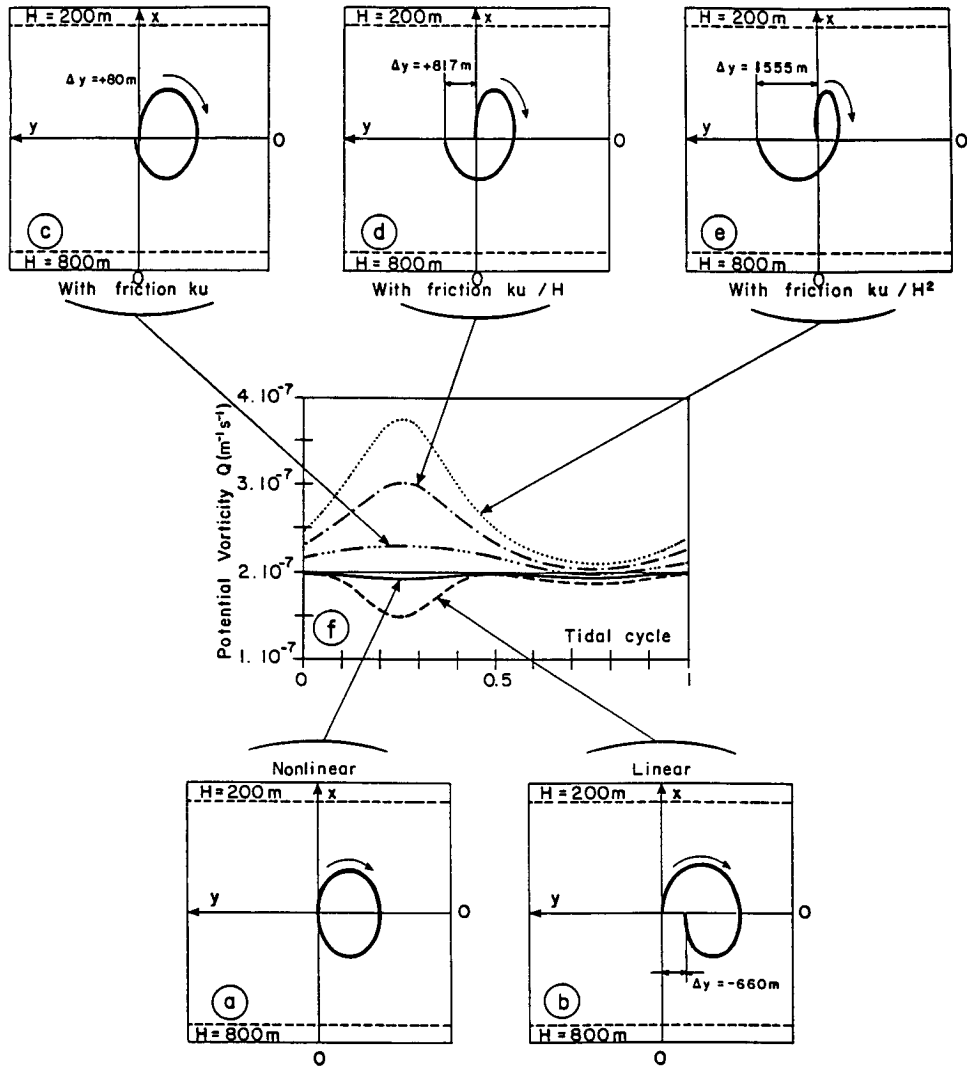

FIG. 5. Lagrangian trajectories resulting from the frictionless nonlinear model (a), from the linear model (b), and from the nonlinear theories using a weak friction ($k \to 0$) in three cases (c), (d), and (e). The behavior of the potential vorticity along the trajectory is in each case presented in (f). Only in the first model (a) is the potential vorticity conserved and the trajectory a closed curve.

transport along the slope. The associated potential vorticity is nearly constant (Fig. 5f):

$$Q^* \approx \frac{f}{H(x_0)} = 2 \times 10^7 \text{ m}^{-1} \text{ s}^{-1}.$$

Conservation of Q^* is only approximate because we have made many assumptions. Nevertheless, this vorticity behavior validates the whole analytical model. A comparison with the linear approximation (Fig. 5b) and with tidal rectification theories using a friction law (Fig. 5c,d,e) is very instructive. The linear trajectory shows a negative Lagrangian current along the slope and conservation of potential vorticity is poor. In the case of weak friction, three laws (ku; ku/H; ku/H^2) are considered and in each case, according to Loder (1980), a positive Lagrangian y transport is observed. For $\tau = ku/H$ and $\tau = ku/H^2$, the potential vorticity conservation is very poor, showing that the Huthnance (1973) and the Loder (1980) procedures are, for weak friction, unable to conserve the potential vorticity. With a linear friction law, ($\tau = ku$), the proposed solution is more efficient, but the form of the y component of the residual current is identical with that obtained by truncation of our nonlinear solution (when only the first f_i function is conserved).

4. Application to the A'–A transect

a. Method

The method mentioned above is similar to a perturbation method. The convergence criterion shows

the limit beyond which nonlinear terms become dominant with respect to the others. On the A'–A transect, since the ratio L_M/L_T is less than 1 (Fig. 2), the nonlinearities are sufficiently weak for us to assume that nonlinear effects are only a perturbation of the linear tide. For natural topographies the results are not a simple mathematical function as for a constant slope, so convergence should be numerically checked and the x^* expansion truncated.

Assuming, at the top of the slope, a linear tidal current described by A_9 and A_8, we can separate time and space variables of the f_i functions in the following way:

$$f_i(x, t) = g_i(x)[\sin(\omega t)]^{i+1},$$

where

$$g_0 = -\frac{H_d u_d}{\omega H(x)}$$

$$g_{i+1} = -\frac{H_d u_d}{(i+1)\omega H(x)} \frac{dg_i(x)}{dx}.$$

The derivatives are evaluated in terms of finite differences

$$\frac{dg_i(x)}{dx} \approx \frac{g_i\left(x + \frac{1}{2}\Delta x\right) - g_i\left(x - \frac{1}{2}\Delta x\right)}{\Delta x}.$$

Space derivatives of depth appear in these expressions. A linear interpolation of those along the transect is inefficient because the derivatives are either discontinuous or undefined at various tabulated depths. A cubic spline interpolation is performed and only the three first terms in the x^* expansion are retained:

$$x^* = x + f_0(x, t) + f_1(x, t) + f_2(x, t).$$

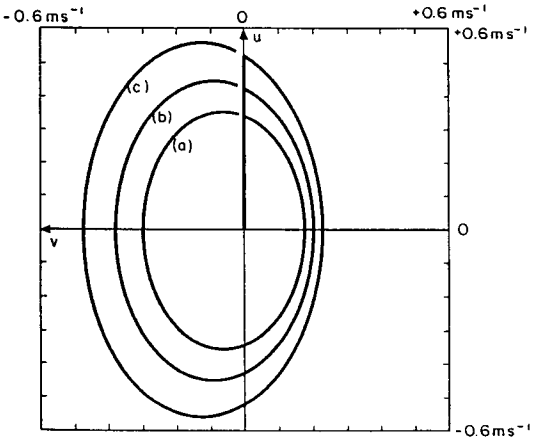

FIG. 6. Nonlinear tidal current ellipses at the top of the shelf break (near P_1) for three mass transport amplitudes: (a) $H_d u_d = 70$ m^2 s^{-1}; (b) $H_d u_d = 87$ m^2 s^{-1}; (c) $H_d u_d = 104$ m^2 s^{-1}.

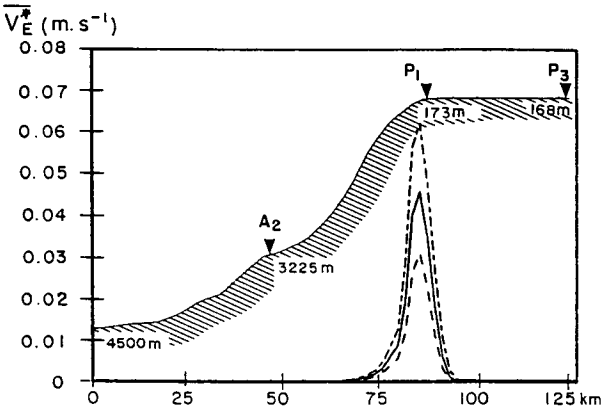

FIG. 7. Residual Eulerian current $\overline{v_E^*}$ profile computed along the cross section A'–A for the three various situations: $H_d u_d = 70$ m^2 s^{-1} (dotted); $H_d u_d = 87$ m^2 s^{-1} (solid); $H_d u_d = 104$ m^2 s^{-1} (chain-dotted). The maximum of tidal rectification current is in the vicinity of P_1.

Using A_8 and A_9 for the linear currents and Eq. (11) allows the nonlinear behavior of tidal currents to be derived.

b. Results

Tidal currents observed at P_1 are close to 0.5 m s^{-1}. They reach 0.6 m s^{-1} at spring tide and decrease to 0.4 m s^{-1} at neap tide. Since the depth is 173 m, the mass flux amplitudes are, respectively, $H_d u_d = 87$ m^2 s^{-1}, $H_d u_d = 104$ m^2 s^{-1} and 70 m^2 s^{-1}. Nonlinear tidal current hodographs in these three situations are presented for a depth of 200 m (Fig. 6). As for a Poincaré wave in the Northern Hemisphere, the oscillating current rotates clockwise. The hodograph is strongly asymmetric with respect to the u axis, and thus an Eulerian mean current, with the shallower depth to its right, occurs. A numerical time integration over one tidal period of v^* is used to evaluate the residual current $\overline{v^*}$ along A'–A. The range of this parameter lies between 0.03 m s^{-1} and 0.07 m s^{-1} with a maximum value at the shelf break (Fig. 7). The mooring P_1 is in the vicinity of the maximum. The predicted mean current is somewhat underestimated at P_1. The very sharp decrease in mean velocity over the shelf reproduces the magnitude gap between P_1 and P_2. Of course, at A_2 (H = 3 225 m) the observed weak mean current (0.03 m s^{-1}) is not a consequence of nonlinear advective effects. An example of a water column trajectory is presented (Fig. 8) in the region where greatest nonlinearities are estimated. Tidal displacement over one tidal period is nearly a closed curve. Moreover, mean Lagrangian current is found (10^{-3} m s^{-1}) to be insignificant.

Efficiency of the method is checked by the potential vorticity conservation Q^*. In the worst case, $\Delta Q^*/Q^*$ equals about 11%. Potential vorticity becomes constant if the trajectory is computed using the linear current

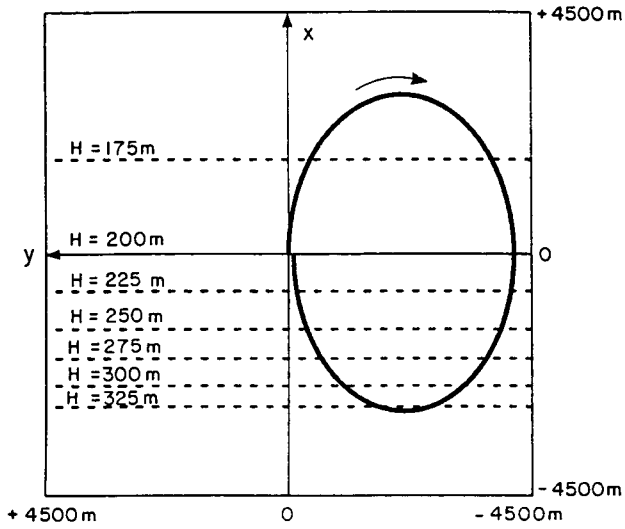

FIG. 8. Lagrangian trajectory for a water column located at the top of the shelf edge at time $t = 0$. Despite an irregular slope, the displacement is symetrical to the starting isobath.

u and the nonlinear current v^*. Thus, the aforedescribed solution of the nonlinear set of equations (3) [after transformation by (10)] is exact. Therefore, the bias comes from poor approximation of the cross-isobath current in the linearized advective terms. To improve the method, a better approximation for $u^*(\partial/\partial x)$ as $u(\partial/\partial x)$ must be taken. A convenient way is to consider the truncated nonlinear cross-isobath current u_1 obtained by the approximation $u(\partial/\partial x)$ and to evaluate the linearized self-advection by $u_1(\partial/\partial x)$

$$u_1 = \frac{H_d u_d \cos(\omega t)}{H[x - (H_d u_d/\omega H)\sin(\omega t)]}$$

or

$$u_1 = \frac{H_d u_d}{H(x)}\cos(\omega t)\left(1 + \frac{H_d u_d}{\omega H^2}\frac{dH(x)}{dx}\sin(\omega t)\right).$$

Although evaluation of f_i functions is lengthy, the vorticity conservation is significantly improved ($\Delta Q^*/Q^* < 2\%$). In all cases, the behavior of parcel displacement and residual motion is unaltered by the new approximation. Thus, vorticity conservation is an accurate check on the validity of the result.

c. *Nonlinear interaction between M_2 and S_2*

It is well known that the linear sum of two waves of different frequencies generates a "beat" phenomenon. This appears in the spring tide to neap tide cycle. When we consider the two semidiurnal waves M_2 ($\omega_{S_2} = 1.405 \times 10^{-4}$ s^{-1}) and S_2 ($\omega_{S_2} = 1.454 \times 10^{-4}$ s^{-1}) and when the nonlinearities are nonnegligible, two forced oscillations are expected. The first is the MS_4 component (of frequency $\omega_{M_2} + \omega_{S_2}$). The second is the MS_f component of the tide that appears in the form of a fortnightly modulation of the mean current (here integrated over one tidal period). In fact, if only the effect of M_2 and S_2 over a slope are considered, three contributions to low-frequency motion occur simultaneously. These are self-interactions of each wave (M_2 or S_2), which generate a purely residual current and cross-interaction between M_2 and S_2, which induces a fortnightly oscillating current. Of course, linear approximation of tidal current is a linear sum of the M_2 and S_2 contribution:

$$u(x, t) = \frac{1}{H(x)}([H_d u_d]_{M_2}\cos(\omega_{M2}t) + [H_d u_d]_{S_2}\cos(\omega_{S2}t))$$

$$v(x, t) = -\frac{f}{\omega}\frac{1}{H(x)}([H_d u_d]_{M_2}\sin(\omega_{M2}t) + [H_d u_d]_{S_2}\sin(\omega_{S2}t)). \quad (19)$$

Using (19) to calculate the x^* transformation (14) we obtain the nonlinear current:

$$u^*(x, t) = u(x^*, t)$$
$$v^*(x, t) = v(x^*, t).$$

These results are represented in Fig. 9 for the transect A'–A at 200-m depth. Comparison of the linear (u) and the nonlinear (u^*) cross-isobath currents shows that the latter is slightly stronger in amplitude. No residual cross-isobath current is generated. Along the shelf break the v^* current is strongly asymmetrical, and consequently a residual and a fortnightly oscillating current occurs. The magnitude of this low-frequency current varies from 0.08 m s^{-1} at spring tide to 0.02 m s^{-1} at neap tide. Thus, amplitude of the MS_f component of the current along the isobath is close to 0.03 m s^{-1}.

5. Conclusions and summary

It is shown that nonlinear dynamics of an inviscid ocean are sufficient to construct a rectification mechanism because the dynamics over a slope are nonlinear, even if friction vanishes. In this study, we have described a simple alternative method that to harmonic separation and truncation. Our results are in agreement with potential vorticity conservation, and the trajectory of a water column is a closed ellipse. For tidal currents rotating anticyclonically in the Northern Hemisphere, the mean Eulerian current flows along the slope leaving the shallow water on the right-hand side.

The most important result is the absence of mass transport along the isobaths. The Eulerian residual current cancels the Lagrangian mean current due to the linear approximation. This result improves the work of Moore (1973), which had demonstrated that Lagrangian transport generated by a wave over a non-

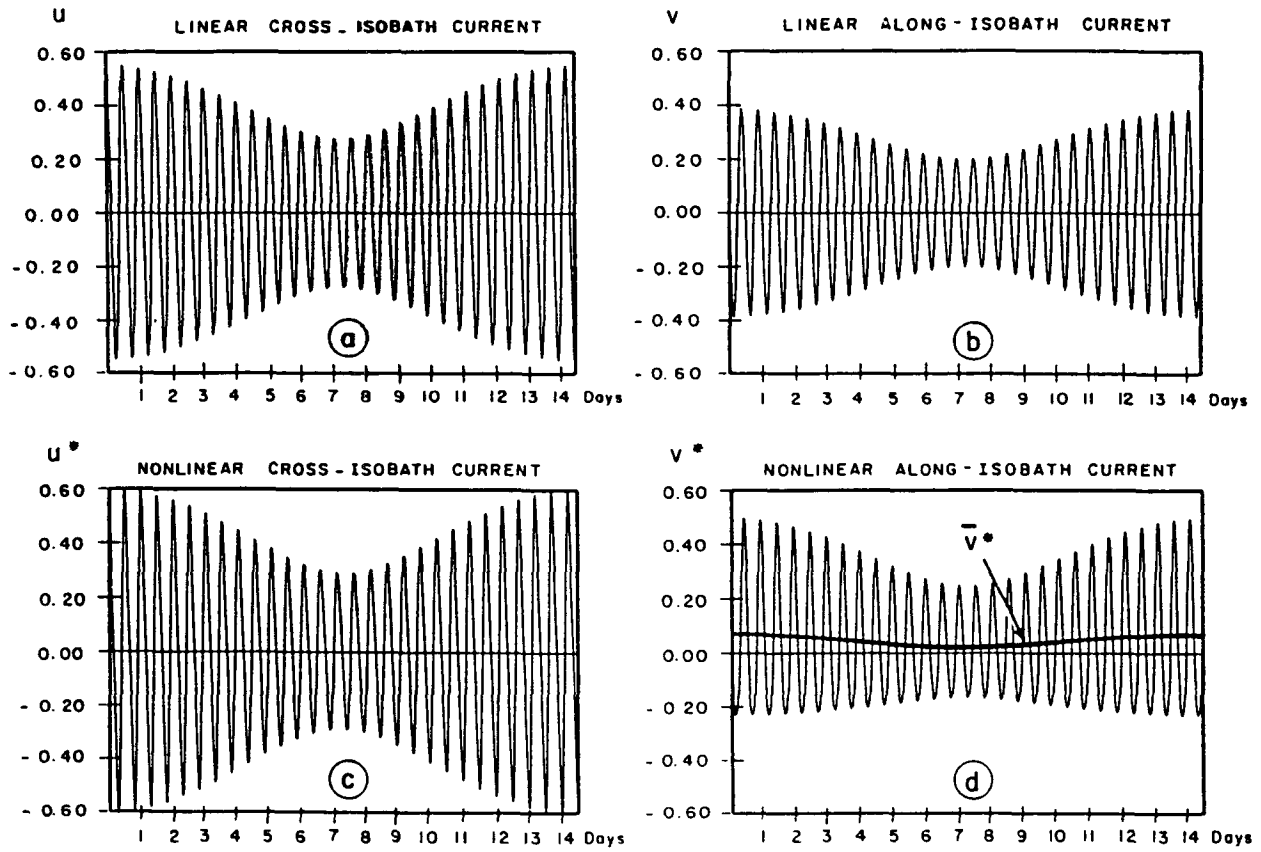

FIG. 9. The linear sum of tidal waves M_2 and S_2 just shows the beating of these two respective components. No residual current is generated (a), (b). Introduction of nonlinear interaction increases the current amplitude perpendicular to the isobath (c). Along the y axis, residual, as well as 14.7-day oscillating and semidiurnal, currents are generated (d).

flat bottom must follow the geostrophic contours (f/H = const). Consequently, if the domain boundaries intersect the latter contours, the mean Lagrangian current vanishes. A rectilinear shelf break considered here is, in fact, a closed geostrophic contour. It is shown that in such a case also no mass transport occurs.

An application to a particular transect across the slope of the Bay of Biscay is in agreement with the analytical results. Data and calculations are in the same range. Thus, the tidal rectification process generates the greatest part of the observed residual current at the top of the slope. The nonlinear interaction between the semidiurnal lunar component (M_2) and solar component (S_2) is correctly reproduced.

The weakness of analytical results that use friction in order to remove geostrophic degeneracy is evident, but the physical concept (a distortion in the vorticity advection due to friction) is basically sound. The bias comes from taking into account, in the forcing term of the residual momentum equation, the linear currents (perturbed by friction) instead of nonlinear (also perturbed by friction) currents. The feedback of the generated residual currents to the tidal velocity field introduced by Loder (1980) improves the theory, but probably remains insufficient to describe the complete nonlinear behavior of the tide. An interesting challenge is an extension of the pseudo-Lagrangian method developed here in order to examine the momentum balance with friction.

Acknowledgments. Financial support was provided by contract from Direction des Recherches et Etudes Techniques and from Etablissement Principal du Service Hydrographique et Oceanographique de la Marine, Ministry of Defence, Paris. The authors are indebted to Annie Mevel and John Love for help with the English text and P. Doare for the figure drawing.

APPENDIX A

Linear Tide over a Slope

When a normal incident tidal wave over a shelf break is considered, two mathematical (and physical) approaches are possible. In the first, the free-surface behavior over the slope can always be expressed as

$$\tilde{\zeta}(x, t) = \zeta_0[F(x, \omega)\cos(\omega t) + G(x, \omega)\sin(\omega t)], \quad \text{(A1)}$$

where $F(x, \omega)$ and $G(x, \omega)$ are time-independent functions. This is an alternative expression of the more conventional description of a progressive wave

$$\tilde{\zeta}(x, t) = \zeta(x, \omega) \cos[\omega t + \varphi(x)]$$

where the amplitude is

$$\zeta(x, \omega) = \zeta_0(F^2 + G^2)^{1/2},$$

and the phase is

$$\varphi = \arctan\left(\frac{G}{F}\right).$$

Equation (A1) describes only a linear tide. Using (A1) and the linearized equations of motion, the current components are expressed in terms of F and G derivatives

$$\tilde{u} = \frac{g\zeta_0\omega}{(\omega^2 - f^2)}\left[\frac{dG}{dx}\cos(\omega t) - \frac{dF}{dx}\sin(\omega t)\right] \quad \text{(A2)}$$

$$\tilde{v} = \frac{g\zeta_0 f}{(\omega^2 - f^2)}\left[-\frac{dF}{dx}\cos(\omega t) - \frac{dG}{dx}\sin(\omega t)\right]. \quad \text{(A3)}$$

Therefore an alternative form of the propagation equation is the system:

$$\frac{d^2F}{dx^2} + \frac{1}{H}\frac{dH}{dx}\frac{dF}{dx} + \frac{\omega^2 - f^2}{gH}F = 0 \quad \text{(A4)}$$

$$\frac{d^2G}{dx^2} + \frac{1}{H}\frac{dH}{dx}\frac{dG}{dx} + \frac{\omega^2 - f^2}{gH}G = 0. \quad \text{(A5)}$$

In the case of a progressive wave Eqs. (A1)–(A3) allow calculation of the mean energy flux along the x axis:

$$\bar{\phi}_U = \rho g H \overline{\tilde{\zeta}\tilde{u}}$$

$$\bar{\phi}_U = \frac{1}{2}\frac{\rho g^2\zeta_0^2 H\omega}{(\omega^2 - f^2)}\left(F\frac{dG}{dx} - G\frac{dF}{dx}\right). \quad \text{(A6)}$$

Using (A2), (A3) gives

$$\overline{\tilde{u}\frac{\partial\tilde{v}}{\partial x}} = \frac{1}{2}\frac{g^2\zeta_0^2 f\omega}{(\omega^2 - f^2)^2}\left[\frac{dF}{dx}\frac{d^2G}{dx^2} - \frac{dG}{dx}\frac{d^2F}{dx^2}\right].$$

Calculating dF/dx (A5) $- dG/dx$ (A4) $= 0$, we obtain

$$\left[\frac{dF}{dx}\frac{d^2G}{dx^2} - \frac{dG}{dx}\frac{d^2F}{dx^2}\right] = \frac{(\omega^2 - f^2)}{gH}\left(G\frac{dF}{dx} - F\frac{dG}{dx}\right)$$

and finally:

$$\overline{\tilde{u}\frac{\partial\tilde{v}}{\partial x}} = \frac{1}{2}\frac{\rho g^2\zeta_0^2\omega f}{(\omega^2 - f^2)H}\left(F\frac{dG}{dx} - G\frac{dF}{dx}\right)$$

$$\overline{\tilde{u}\frac{\partial\tilde{v}}{\partial x}} = f\frac{\bar{\phi}_U}{\rho g H^2}. \quad \text{(A7)}$$

In the second approach and according to the weakness of the local divergence parameter, the continuity equation leads to

$$u(x, t) = \frac{H_d u_d}{H(x)}\cos(\omega t). \quad \text{(A8)}$$

For a normal incident wave, it is

$$v(x, t) = -\frac{f}{\omega}\frac{H_d u_d}{H(x)}\sin(\omega t). \quad \text{(A9)}$$

Knowledge of the current u_d in the deeper region (depth $= H_d$) is sufficient to describe the velocity component u and v at any point over the slope. Note that these approximations transform a progressive wave into a standing one.

APPENDIX B

Case of Constant Slope

Knowledge of the linear cross-isobath current (15) allows one to clearly make the x^* expansion and the f_i function defined [using (14)] as

$$\frac{\partial f_0}{\partial t} = -u, \quad \text{thus} \quad f_0 = -\frac{H_d u_d}{\omega H(x)}\sin(\omega t)$$

$$\frac{\partial f_1}{\partial t} = -u\frac{\partial f_0}{\partial x}, \quad \text{thus} \quad f_1 = +\frac{1}{2}\frac{a}{H}\left(\frac{H_d u_d}{\omega H}\right)^2 \sin^2(\omega t).$$

Finally

$$f_i = (-1)^{i+1}\frac{1\cdot 3\cdot 5\cdots[2(i+1)-3]}{(i+1)!} \times \left(\frac{a}{H}\right)^i\left(\frac{H_d u_d \sin(\omega t)}{\omega H}\right)^{i+1}.$$

The potential vorticity equation and the nondivergence x transport at the tidal frequency allows elimination of the constant (with respect to t) that can appear in the time integration. The nonlinear current is derived from the linear one by (11), giving

$$u^* = \frac{H_d u_d \cos(\omega t)}{H(x)(1 + S)}$$

$$v^* = -\frac{f}{\omega}\frac{H_d u_d \sin(\omega t)}{H(x)(1 + S)},$$

where S is the series

$$S = \frac{Z}{2} + \frac{\frac{1}{2}\left(\frac{1}{2} - 1\right)}{2!}Z^2 + \cdots + \frac{\frac{1}{2}\left(\frac{1}{2} - 1\right)\cdots\left(\frac{1}{2} - n + 1\right)}{n!}Z^n + \cdots$$

with

$$Z = \frac{2a}{\omega}\frac{H_d u_d}{H^2}\sin(\omega t).$$

The series $(1 + S)$ is a known binomial series, which converges to $(1 + Z)^{1/2}$ for $|X| \leqslant 1$. Thus, the nonlinear currents are rewritten

$$\left.\begin{aligned} v^*(x, t) &= -\frac{f}{\omega}\frac{H_d u_d \sin(\omega t)}{H(x)(1+Z)^{1/2}} = \frac{v(x,t)}{(1+Z)^{1/2}} \\ u^*(x, t) &= \frac{H_d u_d \cos(\omega t)}{H(x)(1+Z)^{1/2}} = \frac{u(x,t)}{(1+Z)^{1/2}} \end{aligned}\right\}.$$

The convergence of the $(1 + S)$ series is, in fact, obtained by the unequality

$$\frac{2aH_d u_d}{\omega H^2} \leqslant 1.$$

Using (1) and (2), an equivalent convergence condition is expressed in terms of physics by sufficiently small nonlinearity:

$$\frac{2L_M}{L_T} \leqslant 1.$$

REFERENCES

Huthnance, J. M., 1973: Tidal current asymmetries over the Norfolk sandbanks. *Estuar. Coastal Mar. Sci.*, **1,** 89–90.

——, 1981: On mass transport generated by tides and long waves. *J. Fluid Mech.*, **102,** 367–387.

Loder, J. W., 1980: Topographic rectification of tidal currents on the sides of Georges Bank. *J. Phys. Oceanogr.*, **10,** 1399–1416.

Longuet-Higgins, 1969: On transport of mass by time-varying ocean currents. *Deep-Sea Res.*, **16,** 431–447.

Maas, L. R. M., J. T. F. Zimmerman, and N. M. Temme, 1987: On the exact shape of the horizontal profile of a topographically rectified tidal flow. *Geophys. Astrophys. Fluid Dyn.*, **38,** 105–129.

Moore, D., 1970: The mass transport velocity induced by free oscillations at a single frequency. *Geophys. Fluid Dyn.*, **1,** 237–247.

Pedlosky, J., 1979: *Geophysical Fluid Dynamics.* Springer-Verlag. 624 pp.

Pichon, A., and R. Maze, 1990: Internal tides over a shelf break: Analytical model and observations. *J. Phys. Oceanogr.*, **20,** 658–671.

Pingree, R. D., and L. Maddock, 1979: Tidal flow around an island with a regularly sloping bottom topography. *J. Mar. Biol. Ass. U. K.*, **59,** 699–710.

——, and ——, 1980a: The effects of bottom friction and earth's rotation on an island's wake. *J. Mar. Biol. Ass. U. K.*, **60,** 499–508.

——, and ——, 1980b: Tidally induced residual flows around an island due to both frictional and rotational effects. *Geophys. J. Roy. Astron. Soc.*, **63,** 533–546.

——, and G. T. Mardell, 1987: Tidal flows around the channel islands. *J. Mar. Biol. Ass. U. K.*, **67,** 691–707.

——, and B. Lecann, 1989: Celtic and Armorican slope and shelf residual currents. *Progress in Oceanography,* Vol. 23, Pergamon, 303–338.

Rhines, P. B., 1977: The dynamics of unsteady currents, chapter 7. *The Sea,* Vol. 6, Wiley Interscience,

Robinson, I. S., 1981: Tidally vorticity and residual circulation. *Deep-Sea Res.*, **28A**(3), 195–212.

——, 1983: Tidally induced residual flows. *Physical Oceanography of Coastal and Shelf Seas,* B. Johns, Ed., Elsevier Oceanogr. Ser., 321–356.

Wright, D. G., and J. W. Loder, 1988: On the influences of nonlinear bottom friction on the topographic rectification of tidal currents. *Geophys. Astrophys. Fluid Dyn.*, **42,** 227–245.

Zimmerman, J. T. F., 1979: On the Euler–Lagrange transformation and the Stokes' drift in the presence of oscillatory and residual currents. *Deep-Sea Res.*, **26A,** 505–520.

——, 1980: Vorticity transfer by tidal currents over an irregular topography. *J. Mar. Res.*, **38**(4), 601–630.

——, 1981: Dynamics, diffusion, and geomorphological significance of Tidal residual eddies. *Nature,* **290,** 549–555.